Available online at www.sciencedirect.com
SCIENCE DIRECT®
Tectonophysics 370 (2003) 227–239
TECTONOPHYSICS
www.elsevier.com/locate/tecto

Effects of reaction kinetics and fluid drainage on the development of pore pressure excess in a dehydrating system

Wei-Hau Wang[a,*], Teng-fong Wong[b]

[a] *Institute of Applied Geophysics, National Chung Cheng University, 160 Sanshin, Minghsiung, Chiai 201, Taiwan, ROC*
[b] *Department of Geosciences, State University of New York at Stony Brook, Stony Brook, NY 11794-2100, USA*

Accepted 31 March 2003

Abstract

Fluid is released by dehydration reactions during prograde metamorphism. If the Claperyron slope for the dehydrating reaction is positive, then there is a net decrease in the total solid volume, which implies an irreversible increase in porosity. If the dilation of the pore space is insufficient to provide storage for all the released fluid, then pore pressure excess is generated, and if it becomes sufficiently high, it may lead to brittle fracturing. The time scale for pressure generation and the pore pressure excess can be maintained over long duration hinge on the interplay of reaction kinetics and fluid drainage. Motivated by experimental and microstructural observations, a hydrological model is developed that incorporates dehydration kinetics and its pressure dependence. Analytic solutions were derived for the undrained development of pore pressure. Whether lithostatic pressure may be exceeded hinges on magnitude of the overstep in temperature and corresponding equilibrium pressure. The time scale for development of pore pressure depends on the trade-off between poroelasticity and the pressure sensitivity of reaction rate. A finite difference model was also developed to simulate the progressive development of pore pressure excess, dehydration and porosity development. The model captures the experimental observation in gypsum of a reaction front that progressively propagates from the drained end toward the undrained end of a laboratory sample. It is also in reasonable agreement with experimental data on fluid drainage and porosity production.

Keywords: Reaction kinetics; Pore pressure excess; Dehydration; Gypsum

1. Introduction

Fluids exert significant mechanical and chemical effects on tectonic processes. Numerous mechanisms for the generation and maintenance of overpressure in sedimentary, metamorphic and tectonic processes have been identified, and their consequences on various mechanical and geochemical processes have been analyzed (Bredehoeft and Hanshaw, 1968; Domenico and Palciauskas, 1988; Bredehoeft and Norton, 1990; Ingebritsen and Sanford, 1998). An important mechanism is the decomposition of hydrous minerals during prograde metamorphism, which was underscored in the seminal studies of Raleigh and Paterson (1965) on serpentinite and Heard and Rubey (1966) on gypsum.

The experimental data showed that dehydration provides a viable mechanism for weakening and

* Corresponding author. Tel.: +886-5-2720411x66206; fax: +886-5-2720807.
E-mail address: seiwhwg@eq.ccu.edu.tw (W.-H. Wang).

0040-1951/03/$ - see front matter © 2003 Elsevier B.V. All rights reserved.
doi:10.1016/S0040-1951(03)00188-4

embrittlement, which may facilitate overthrusting, as well as seismicity and magma generation in a subduction environment. Serpentinite dehydration is often considered to be a mechanism for earthquakes at intermediate depth (Kirby et al., 1996; Peacock, 2001). Since anhydrite is sometimes found along the decollement, the dehydration of gypsum to anhydrite has been cited as a mechanism for overthrusting (Hanshaw and Bredehoeft, 1968). At shallower depths, clay dehydration is considered to play important roles in influencing the dynamics of sedimentary formations and accretionary prisms (Moore and Vrolijk, 1992).

To dramatize the weakening, the early experimental studies were conducted under undrained conditions. With the onset of dehydration, the massive release of fluid is trapped within the pore space since the sample assemblage is completely encapsulated. As far as relating the rock mechanics data to crustal processes, these undrained experiments suffer from two shortcomings. First, one does not have access to the interior of the completely encapsulated sample, and therefore the evolution of relevant hydromechanical attributes cannot be monitored. Second, these data are relevant only to a dehydrating layer embedded in a perfectly impermeable rock without any drainage of fluid.

To investigate how dehydration and fluid transport are coupled and to address the question whether such a weakening mechanism is viable under drained conditions in the Earth, Ko et al. (1997) conducted detailed studies of gypsum dehydration under both drained and undrained conditions, and Wong et al. (1997) developed a hydrologic model that captures some of the key laboratory observations. While the theoretical model elucidates the feedback of fluid drainage on the development of pore pressure excess in a dehydrating system, it has two limitations. First, the reaction kinetics is modeled in a somewhat simplistic manner assuming a constant rate. More realistic kinetics have been incorporated in recent studies (Connolly, 1997; Ague et al., 1998; Balashov and Yardley, 1998), which indicate that the interplay of reaction kinetics and fluid flow may result in complex development of pore pressure excess. Second, detailed microstructural observations on dehydrated samples indicate significant spatial heterogeneity. In particular, Stretton (1996) and Miller et al. (2003) documented the progressive development of a "reaction front" in a gypsum sample undergoing dehydration, a phenomenon that cannot be reproduced in the previous model.

The primary goal of this study is to develop a more comprehensive model that accounts for both reaction kinetics and fluid transport and can capture the spatial heterogeneity as manifested by the progressive development of a reaction front. The finite difference technique was used, and analytic estimate of the time scale of pore pressure development was also derived. The theoretical predictions are compared with experimental and microstructural data, and tectonic implications of our model in relation to overpressure generation and mechanical instability are also discussed.

2. Dehydration kinetics and governing equations for pore pressure development

We will consider a porous medium that is initially at hydrostatic equilibrium with pore pressure $P_f = P_0$ (Fig. 1). With the initiation and development of dehydration, the spatiotemporal evolution of the pore pressure excess P' $(= P_f - P_0)$ is governed by the hydraulic diffusion equation that was first proposed

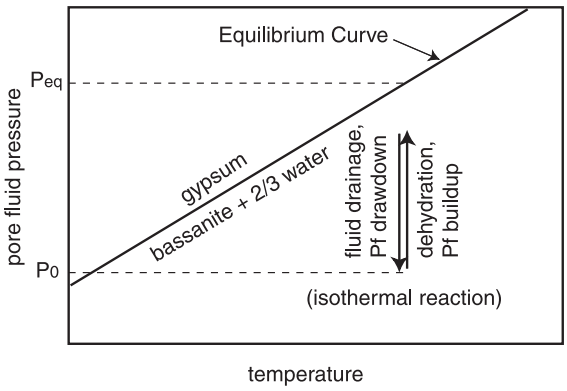

Fig. 1. Schematic diagram showing pore fluid pressure generation or dissipation during isothermal dehydration. The transformation of gypsum to bassanite, which has a positive Claperyron slope, is used to demonstrate the effects of reaction kinetics under undrained condition. All our models have an initial pore fluid pressure P_0 and would never exceed the pore fluid pressure at equilibrium P_{eq}. Refer to text for details.

by Walder and Nur (1984) and modified by Wong et al. (1997) with the addition of a fluid source term:

$$\phi(\beta_\phi + \beta_f)\frac{\partial P'}{\partial t} = \nabla\cdot\left(\frac{\kappa}{\mu}\nabla P'\right) + \dot{\Gamma} - \dot{\Phi}, \quad (1)$$

where ϕ is the interconnected porosity; β_ϕ is the pore compressibility; β_f is the fluid compressibility; κ is the permeability; μ is the viscosity of the fluid; $\dot{\Gamma}$ is the dehydration rate (defined as the volume of water released per unit bulk rock volume per unit time); and $\dot{\Phi}$ is the irreversible porosity production rate.

One of the major differences between this study and that of Wong et al. (1997) is that the dehydration rate $\dot{\Gamma}$ is no longer assumed to be a constant. Laboratory measurements in gypsum (Ko et al., 1997) and other petrological studies indicate that $\dot{\Gamma}$ decreases with increasing pore pressure. Such kinetics of dehydration can be described by a general rate law (Lasaga and Rye, 1993):

$$\dot{\Gamma} = Mc\bar{A}s\,|\,\Delta G\,|^N, \quad (2a)$$

with

$$\Delta G = \Delta V\,\mathrm{d}P_f - \Delta S\,\mathrm{d}T, \quad (2b)$$

or

$$\Delta G = a' + b'T + c'P_f + RT\ln f^*_{H_2O} \quad (2c)$$

(Connolly and Cesare, 1993) where M is a reaction-specific stoichiometric constant; c is a temperature-dependent rate constant; $\bar{A}$ is the surface area of the rate-limiting mineral; ΔG is the Gibbs free energy change of the reaction; N is the reaction order; s is $+1$ if ΔG is negative and -1 otherwise; ΔV is the volume change associated with the reaction; ΔS is the entropy change of the reaction; T is temperature; and $f^*_{H_2O}$ is the water fugacity. This rate equation has been adopted in a number of recent studies of pore pressure development induced by dehydration (Connolly, 1997; Ague et al., 1998; Balashov and Yardley, 1998).

In Eqs. (2a)–(2c), the kinetics is sensitively dependent on temperature, with the rate constant c following an Arrhenius law. However, since we will focus here on the hydrological development under isothermal conditions, $\Delta G \approx c'(P_f - P_{eq})$, Eqs. (2a)–(2c) can be simplified as

$$\dot{\Gamma} = \dot{\Gamma}_0\left[\frac{V_{rlm}}{V_{total}}\right]\left[1 - \frac{P_f}{P_{eq}}\right]^N, \quad (3)$$

where $\dot{\Gamma}_0$ is the dehydration rate of the rock with the rate-limiting mineral only at zero pore pressure; V_{rlm}/V_{total} is the volumetric fraction of the rate-limiting mineral to total solid; P_{eq} is the pore pressure at thermodynamical equilibrium. Note that the above equation is based on a simplified assumption that the surface area of the rate-limiting mineral is linearly proportional to V_{rlm}/V_{total}, which is valid if the minerals have approximately the same specific surface area. Unless the reaction kinetics is linear, the reaction order N is expected to be different from unity. Appealing to Lasaga and Rye's (1993) nonlinear kinetic model, Connolly (1997) and Ague and Rye (1999) assumed a value of $N=2.68$ for the reaction orders of chlorite dehydration and CO_2 release from metacarbonates, respectively. For serpentinite dehydration, Ague et al. (1998) empirically determined a value of $N=3.64$ from petrological data.

The spatiotemporal development of pore pressure is coupled to the porosity change as described in Eq. (1) and the following equation (Walder and Nur, 1984):

$$\frac{\partial\phi}{\partial t} = \phi\beta_\phi\frac{\partial P'}{\partial t} + \dot{\Phi}. \quad (4a)$$

If the Claperyron slope for the dehydrating reaction is positive, then there is a net decrease in the total solid volume, which implies an irreversible increase in porosity (Wong et al., 1997; Connolly, 1997). Although it is difficult to independently measure the porosity change, experimental and microstructural data suggest that the dehydration and porosity production rates are positively correlated (Olgaard et al., 1995; Ko et al., 1997). The data indicate an approximately linear relation, but we cannot rule out a nonlinear relation due to the paucity of data. In this study, we will simply assume that the irreversible porosity production rate $\dot{\Phi}$ to be proportional to $\dot{\Gamma}$. In addition, since experimental studies suggest that $\dot{\Phi}$ decreases with increasing effective stress (Ko et al., 1997), we propose here an empirical relation for the irreversible porosity production rate

$$\dot{\Phi} = R(1 - bP_e)\dot{\Gamma}, \quad (4b)$$

where the effective stress P_e is defined to be the difference between the confining pressure P_c and the

pore pressure P_f (i.e., $P_e = P_c - P_f = P_c - P_0 - P'$). The ratio $R = (\dot{\Phi}/\dot{\Gamma})_{P_e} = 0$ is that between the porosity production and dehydration rates at zero effective pressure. The empirical constant b characterizes the irreversible compaction induced by effective pressure. In general, we expect $1 - bP_e > 0$ and the above equation applies for $P_e \geq 0$ before the onset of hydraulic fracturing. As discussed in a later section, we infer from laboratory data for gypsum that $b \sim 5.18 \times 10^{-3}$/MPa (or $1/b \sim 193$ MPa) and $R \sim 0.78$.

During the development of dehydration and pore pressure, poroelastic and irreversible changes in porosity result in concomitant changes in permeability (Ko et al., 1997; Zhang et al., 2000), and therefore the permeability cannot be assumed to be a constant. David et al. (1994) compiled laboratory data and suggested that the permeability κ increases with porosity as a power law, such that

$$\kappa = \kappa_0 \left(\frac{\phi}{\phi_0} \right)^n, \tag{5}$$

where κ_0 and ϕ_0 denote the permeability and porosity at a reference state, respectively. They observed that the exponent n could vary from 1 to 25 in common geologic materials. Recent studies (e.g., Peach and Spiers, 1996; Popp et al., 2001) on permeability in compact rocks further suggested that permeability increases drastically with porosity when porosity is small (<1%). The permeability enhancement becomes more gradual with further increase in porosity. Zhu and Wong (1999) interpreted this phenomenon as the result of two-stage evolution of permeability. At the first stage, permeability increases rapidly in a percolative regime when pore space is only partially connected. Once the connectivity of the pore space has become saturated, which corresponds to a crossover porosity ϕ_c, the permeability and porosity changes follow an approximately linear trend. On the basis of these studies, we adopt a simplified permeability–porosity function as

$$\kappa = \kappa_c \left(\frac{\phi}{\phi_c} \right)^n, \tag{6a}$$

where κ_c is the reference permeability at the crossover porosity ϕ_c, and the exponent n assumes different values in the two different regimes:

$$\begin{cases} n = n_1 & \text{if } \phi \leq \phi_c, \\ n = n_2 & \text{if } \phi \geq \phi_c. \end{cases} \tag{6b}$$

Unlike Walder and Nur's (1984) relation that also reproduces the permeability evolution for the two regimes, Eqs. (6a) and (6b) requires that permeability cannot vanish as long as porosity is finite, but practically, permeability may become so low at very small porosity that it probably cannot be resolved. The advantage of the permeability–porosity relation (Eq. (6a)) is that it is easier to implement in our numerical scheme and seems to fit the experimental observations better.

3. Undrained system: the time scale of overpressure development and potential for hydraulic fracturing

We first consider an undrained dehydrating system that is hydraulically insulated from its surroundings. This corresponds to a laboratory sample that is completely jacketed with an impermeable sleeve, a configuration used in many experimental studies (Heard and Rubey, 1966; Raleigh and Paterson, 1965; Murrell and Ismail, 1976). It also approximates a dehydrating formation embedded within a relatively impermeable rock mass (e.g., shale or compact crystalline rock). Such an undrained scenario was implicitly assumed by Ague et al. (1998) in their analysis of regional metamorphic dehydration and seismic hazard. From a mathematical point of view, this scenario is relatively simple to analyze since one does not need to consider the permeability and Eqs. (6a) and (6b).

Since the boundary condition is homogeneous and initially the hydromechanical properties of the dehydrating material are also homogeneous, the pore pressure excess is uniform within the dehydrating system. At a given location, the evolution of pore pressure excess with respect to time is given by (Wong et al., 1997)

$$\frac{dP'}{dt} = \frac{\dot{\Gamma} - \dot{\Phi}}{\phi(\beta_{\phi+} + \beta_f)}. \tag{7}$$

We will consider the dehydration kinetics described by Eq. (3) above and further assume that the porosity production rate is related to the dehydration rate and effective stress in accordance with Eq. (4b). Under isothermal condition, the difference between the two rates can be evaluated using Eqs. (3) and (4b)

$$\dot{\Gamma} - \dot{\Phi} = C(1 - aP')(P'_{eq} - P')^N, \tag{8a}$$

where C is related to the parameters in Eqs. (3) and (4b) as

$$C = \frac{\dot{\Gamma}_0}{P_{eq}^N}\left(\frac{V_{rlm}}{V_{total}}\right)[1 + R(b(P_c - P_0) - 1)], \tag{8b}$$

and

$$a = \frac{Rb}{Rb(P_c - P_0) - R + 1}. \tag{8c}$$

The pressure excess P'_{eq} is defined by $P'_{eq} = P_{eq} - P_0$. On substituting Eq. (8a) into Eq. (7), we arrive at an equation that describes the evolution of pore pressure:

$$\frac{dP'}{dt} = \frac{C}{\phi(\beta_\phi + \beta_f)}(1 - aP')(P'_{eq} - P')^N. \tag{9}$$

If the reaction kinetics is of first order, then $N = 1$; the above equation can be integrated to give

$$P' = P'_{eq}\frac{1 - \exp[-\bar{B}(1 - aP_{eq}')t]}{1 - aP'_{eq}\exp[-\bar{B}(1 - aP'_{eq})t]}, \tag{10a}$$

where the parameter $\bar{B}$ represents an "effective" modulus averaged over time

$$\bar{B} = \left(\int_0^t C/[\phi(\beta_\phi + \beta_f)]dt'\right)/t. \tag{10b}$$

For $N \neq 1$, the analytic solution of Eq. (9) becomes very complicated and the physical interpretation is not very transparent.

However, for the end-member case $bP_e \ll 1$ (implying that the porosity production rate is independent of the confining and pore pressures), Eq. (9) can be simplified as

$$\frac{dP'}{dt} = \frac{C'}{\phi(\beta_\phi + \beta_f)}(P'_{eq} - P')^N, \tag{11a}$$

with

$$C' = \frac{\dot{\Gamma}_0}{P_{eq}^N}\left(\frac{V_{rlm}}{V_{total}}\right)(1 - R). \tag{11b}$$

It should be noted that even though the porosity production rate is assumed to be pressure-independent here, according to Eq. (4b), the porosity production rate is now proportional to the reaction rate, which does depend on pore pressure according to Eq. (3). The analytic solutions of Eq. (11a) in relatively simple forms can be derived that elucidate the feedback between reaction kinetics and pore pressure development. For the linear case with $N = 1$, if $bP_e \ll 1$, then Eq. (11a) can be integrated to give

$$P_f = P_{eq} - (P_{eq} - P_0)e^{-\bar{B}'t}, \tag{12a}$$

with

$$\bar{B}' = \left(\int_0^t C'/[\phi(\beta_\phi + \beta_f]dt'\right)/t. \tag{12b}$$

The pore pressure grows exponentially from P_0 to the equilibrium value P_{eq} over a characteristic time on the order of $1/\bar{B}'$. For the nonlinear case with $N \neq 1$ and if again we only consider the end-member case such that $bP_e \ll 1$, Eq. (11a) can be integrated to arrive at

$$P_f = P_{eq} - \left[1/(P_{eq} - P_0)^{N-1} + (N-1)\bar{B}'t\right]^{-\frac{1}{(N-1)}}. \tag{12c}$$

The prediction is that the pore pressure will increase with time, approaching the asymptotic value of P_{eq} at time $t \gg 1/[(P_{eq} - P_0)^{N-1}(N-1)\bar{B}']$.

Rapid burial of hydrous rocks can result in concomitant heating and prograde metamorphism and devolatization. The dehydration reaction may therefore develop at pore pressure and temperature conditions that deviate significantly from equilibrium conditions. The equilibrium pressure P_{eq} corresponding to this scenario of "temperature overstepping" (Lasaga and Rye, 1993) can be anomalously high, and in particular, the condition $P_{eq} > P_c$ can occur, in which case, Eq. (12c) predicts that pore pressure can readily increase to attain the condition $P_f > P_c$ necessary for the development of hydraulic fracturing. The implications of these brittle fracture processes for intermediate-depth seis-

micity and subduction-zone magmatism have been elaborated by Etheridge et al. (1984), Kirby et al. (1996) and Davis (1999).

We should note that the model assumptions (that the temperature overstepping occurs under undrained condition and that the porosity production is dependent of effective pressure) behind Eq. (12c) are identical to those adopted by Ague et al. (1998) to analyze regional metamorphic dehydration and seismic hazard. Their prediction for serpentinite dehydration is for overpressure development and periodic hydraulic fracturing to occur in a time scale on the order of 10^3-10^6 years. While Ague et al. (1998) resorted to numerical simulations, we show here that an analytic solution can be derived, which clarifies how the characteristic time scale depends on the reaction kinetics and poroelastic moduli. According to Eq. (12b), the effective modulus $\tilde{B}'$ depends on the elastic properties of the fluid and the rock pore space as well as the porosity. Increasing the porosity or compressibilities (of the pore space and fluid) will decrease $\tilde{B}'$, which according to Eq. (12c) prolongs the characteristic time scale for development of pore pressure excess. Indeed the simulations of Ague et al. (1998) show that an assemblage with initial porosity of 1% requires a significantly longer time scale than another assemblage with 0.1% porosity to build up pore pressure excess. On the other hand, increasing the order of the dehydration reaction or $P_{eq}-P_0$ tends to shorten the characteristic time scale. Indeed the simulations of Ague et al. (1998) show that a larger overstep in temperature (corresponding to a higher value of $P_{eq}-P_0$) accelerates the development of overpressure. It is useful in a future study to specifically infer the parameter values for various dehydrating systems and apply our analysis to regional metamorphism and seismicity following the approach of Ague et al. (1998).

4. Interplay of drainage and dehydration kinetics: spatiotemporal development of pore pressure and reaction front

Although an undrained system represents an idealized scenario, the analysis above underscores the influence of reaction kinetics on the development of pore pressure and potential for hydraulic fracturing. Whether lithostatic pressure may be exceeded hinges on magnitude of the overstep in temperature and corresponding equilibrium pressure. The time scale for development of pore pressure depends on the trade-off between poroelasticity and the pressure sensitivity of reaction rate. Nevertheless, it should be noted that the undrained end-member has its intrinsic limitations. In a more realistic system, the permeability is not zero and therefore the released fluid can drain out and alleviate the pore pressure excess. Furthermore, the porosity production is expected to be sensitive to effective pressure. It is therefore necessary to analyze in more detail the interplay of fluid drainage and reaction kinetics. On one hand, drainage inhibits the rapid development of a pore pressure excess. On the other hand, the more sluggish accumulation of pore pressure allows the reaction to proceed at a faster rate in comparison to the undrained system. Within such a system, the pore pressure and reaction rate cannot be idealized as uniform in space. The problem is more involved and we need to analyze numerically the spatiotemporal development of pore pressure and dehydration.

A one-dimensional finite difference model was employed. We consider boundary and initial conditions identical to those of an ‘‘unconfined dehydrating’’ system as defined by Wong et al. (1997). Unlike this previous study, which assumed the dehydration rate Γ to be constant, here we require it to obey Eq. (3). The laboratory analogy of such an ‘‘unconfined dehydrating’’ system is a cylindrical sample with bottom and surrounding area sealed so that water can only drain from the top of the sample along the symmetry axis. The nominal pore pressure at the drained end is maintained constant. This setup can also be applied to a dehydrating system that is drained from both ends by taking the insulated end as the midplane of the dehydrating layer so that all the hydraulic characters observed in the lower half layer is simply a mirror image of those found in the upper half layer.

Although our approach is quite general, we will mostly focus on the dehydration kinetics of gypsum, since extensive laboratory and microstructural studies (e.g., Olgaard et al., 1995; Stretton, 1996; Ko et al., 1997; Miller et al., 2003) have been done on this system. The dehydration reaction of gypsum to a

metastable phase bassanite can be expressed as follows:

$$CaSO_4 \cdot 2H_2O(\text{gypsum}) \leftrightarrow CaSO_4 \cdot \frac{1}{2}H_2O(\text{bassanite}) + \frac{3}{2}H_2O. \quad (13)$$

In the case of no compaction and complete dehydration, the solid volume change per initial volume of gypsum is -29.3%, and the volume of water released is 37.1% of the initial volume of gypsum. This implies that $(\dot{\Phi}/\dot{I})_{P_e=0} = (29.3/37.1)$ and the maximum increase in porosity can be up to 0.29.

One distinct feature of laboratory measurement is that fluid expulsion from the drained end exhibits three stages: Initially, fluid expulsion was sluggish and followed by an accelerating outflow. At the final stage, fluid expulsion once again dropped to a limited amount as observed at the initial stage except it lasted much longer than the first stage (Olgaard et al., 1995; Ko et al., 1997). We calibrate our model with the data of Ko et al. (1997) for "drained, constant pore pressure" dehydration experiments at a temperature of 128 °C. They employed a polycrystalline gypsum rock from Volterra, Italy, as a starting material. The initial porosity of this rock was approximately 0.5%. This pore space, however, was reduced during pressurization to P_e>40 MPa by closing low-aspect ratio cracks (Ko et al., 1997). For this reason, in this study we assume the initially porosity at the onset of dehydration to be 0.01%. The length of their samples was 25 mm. Here we assume the compressibility β_f and viscosity μ of water to be 2×10^{-10} Pa^{-1} and 2×10^{-4} Pa s^{-1}, respectively. From laboratory measurements, Ko et al. (1997) estimated the pore compressibility β_ϕ to be 5×10^{-9} Pa^{-1}. From petrological

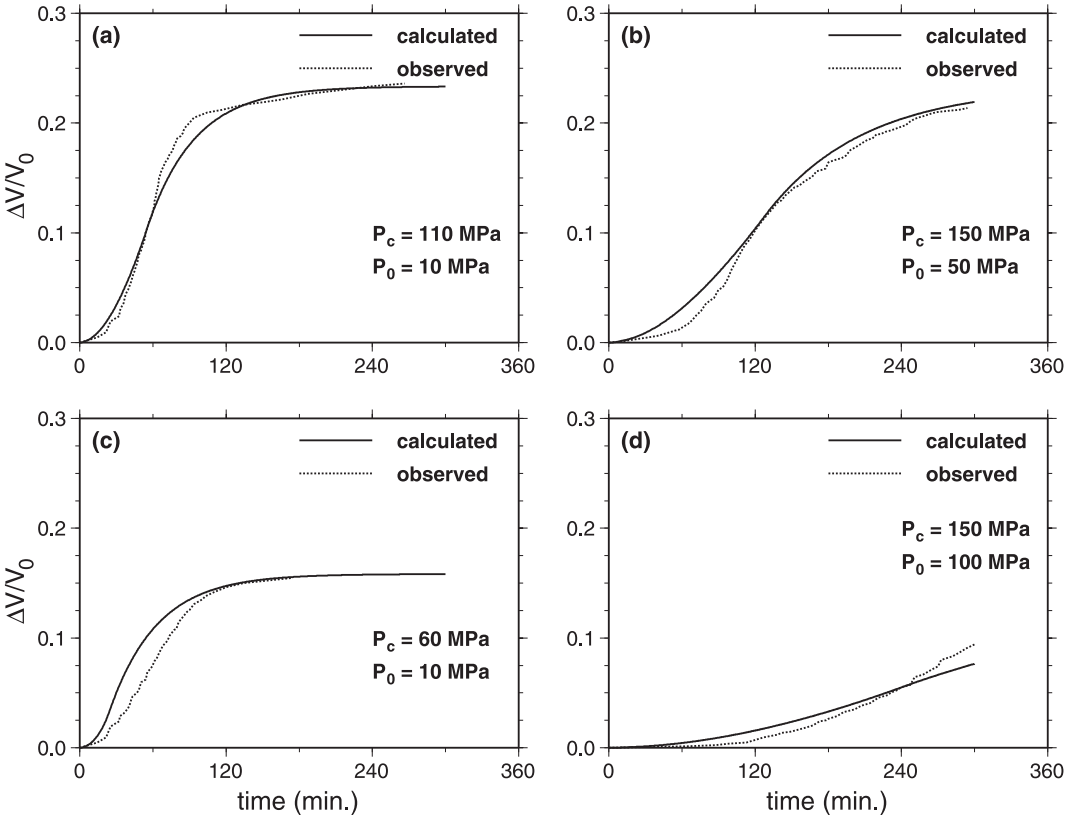

Fig. 2. Comparison of fluid expulsions from experimental observations at $T = 128$ °C (Ko et al., 1997) with those from numerical calculations at various confining pressures and initial pore pressures. The model parameters used for numerical simulations are given in the text. (a) $P_c = 100$ MPa and $P_0 = 10$ MPa; (b) $P_c = 150$ MPa and $P_0 = 50$ MPa; (c) $P_c = 60$ MPa and $P_0 = 10$ MPa; (d) $P_c = 150$ MPa and $P_0 = 100$ MPa.

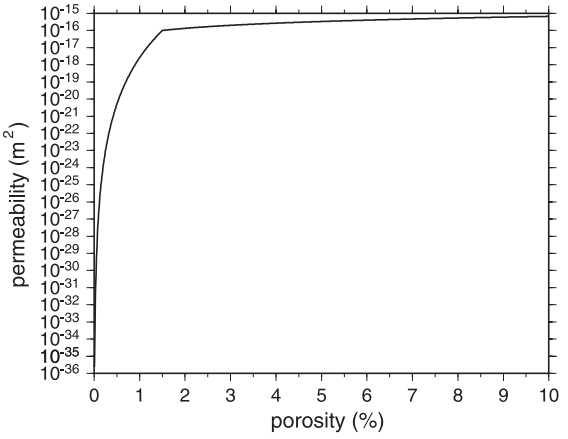

Fig. 3. Empirical relation between permeability and porosity for gypsum.

measurements, P_{eq} at $T=128$ °C is estimated to be about 250 MPa estimated (Murrell, 1985; McConnell et al., 1987).

As shown in Fig. 2, we obtain reasonable agreement between numerical simulations and four sets of experiment data at various confining and initial pore pressures by adopting the following empirical relation (Fig. 3) between permeability and porosity for gypsum:

$$\kappa = 2\times 10^{-16}\left(\frac{\phi}{0.015}\right)^{n},$$

$$\text{with}\begin{cases} n=9, & \text{if } \phi < 1.5\%. \\ n=1, & \text{if } \phi \geq 1.5\%. \end{cases}; \qquad (13a)$$

The dehydration kinetics is assumed to be nonlinear, with $N=4$:

$$\dot{\Gamma} = 1.86\times 10^{-4}\left(\frac{G}{G+B}\right)_V \times\left(1-\frac{P_f}{250}\right)^4, \qquad (13b)$$

and

$$\dot{\Phi} = \frac{29}{37.1}\dot{\Gamma}(1-5.18\times 10^{-3}P_e), \qquad (13c)$$

where $(G/(G+B))_V$ denotes the volumetric fraction of gypsum to total solid with B and G referring to bassanite and gypsum, respectively. Note that in the above empirical equations, κ has the units m^2; $\dot{\Gamma}$ and $\dot{\Phi}$ have the units s^{-1},while P_f and P_e are in MPa.

With the model so calibrated, we can now investigate in more detail the interplay of fluid expulsion, pore pressure excess, percentage of dehydration and porosity changes. The simulations will be compared experiments at $T=128$ °C, $P_c=150$ MPa and $P_0=10$ MPa since this is the condition at which Ko et al. (1997) obtained the most extensive set of laboratory and microstructural data. Fig. 4 illustrates the evolution of the fluid expulsion. Our prediction (the solid line), which agrees well with laboratory data (solid dots), suggests that at stage I (first 20 min after initiation of dehydration), less water flew out of the system. However, during the following 160 min (stage II), fluid expulsion rate increased rapidly. After that, at stage III, the fluid expulsion rate became very small till the reaction was completed.

This distinct evolution of fluid expulsion is comprehensible when we investigate the corresponding pore pressure excess as illustrated in Fig. 5. We find that the initial sluggish fluid expulsion was associated with rapidly elevated pore fluid pressure. This is not a surprise because permeability was so low at this stage that there was little connectivity among pores. As a result, overpressuring by compression of the dehydrating water quickly brought the net pore pressure close to the pore pressure at equilibrium and significantly decelerated the dehydration reaction in most part of the sample. In addition, the increase in pore

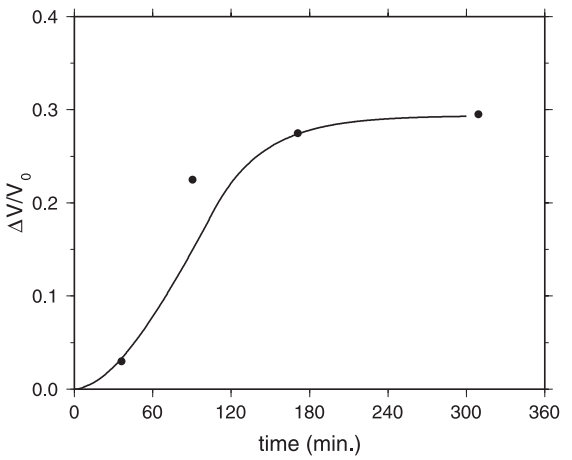

Fig. 4. Temporal evolution of fluid expulsion at $T=128$ °C, $P_c=150$ MPa and $P_0=10$ MPa. The solid dots denote the observed data from Ko et al. (1997) and the solid line is the finite difference calculation.

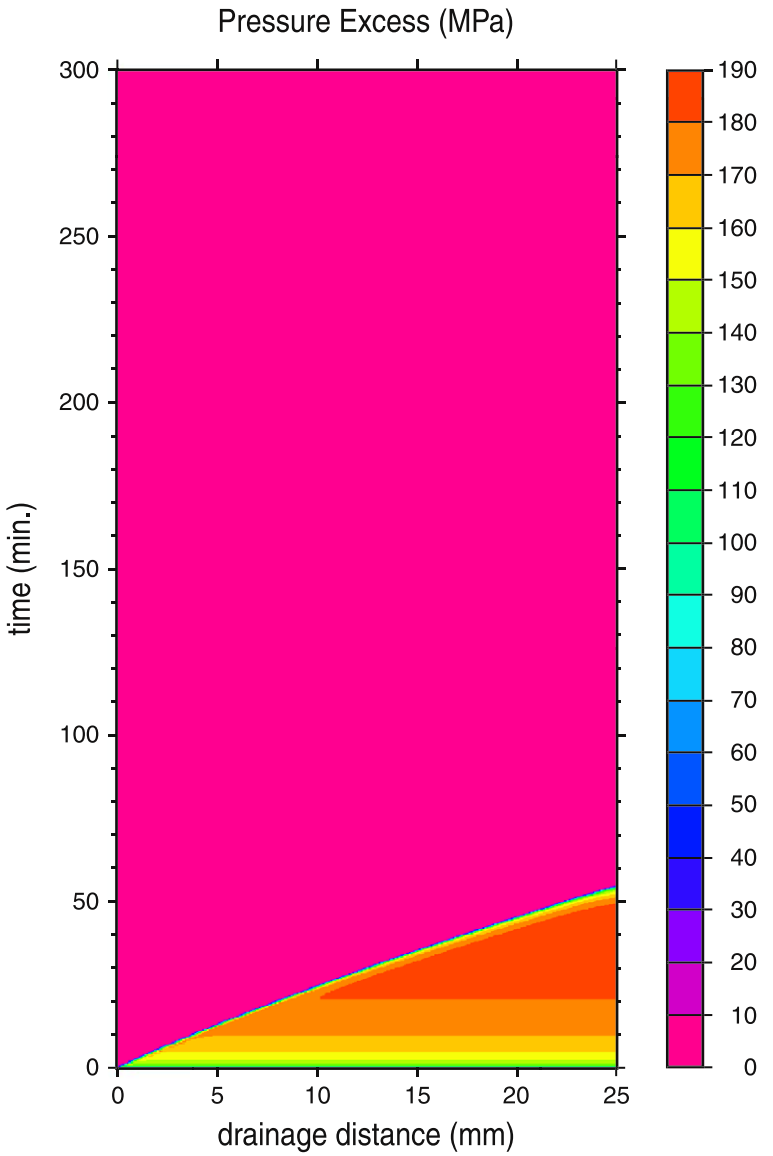

Fig. 5. Spatiotemporal evolution of pore pressure excess at $T = 128$ °C, $P_c = 150$ MPa and $P_0 = 10$ MPa. Pore pressure excess immediately rose to about 150 MPa after the onset of dehydration reaction. Later, the elevated pore pressure gradually released from the drained end (with drainage distance equal zero) toward the sealed end (with drainage distance equal 25 mm).

pressure would lower the effective stress and therefore enhance $\dot{\Phi}/\dot{\Gamma}$ and further reduce the source term, $\dot{\Gamma} - \dot{\Phi}$, in Eq. (1). The low reaction rate and high $\dot{\Phi}/\dot{\Gamma}$ due to elevated pore pressure in poorly permeable gypsum lead to sluggish expulsion at stage I.

It is worth noting that our model predicts that pore pressure at stage I may exceed the confining pressure. If so, hydraulic fracturing might have occurred at this stage. The additional cracks, which have not yet been taken into account in this study, might have reduced some pore pressure shown in Fig. 5 by creating more space to store water and making connections among isolated pores so that the pore fluid could have drained out more easily. The quantitative analysis of

this hydraulic fracturing effect on the dehydration kinetics, however, needs sound knowledge of these cracks such as their growth rates, aspect ratios, orientations and connectivity. Such an analysis is beyond the scope of this study.

The high pore pressure at stage I could have maintained as long as the permeability remained low. As the dehydration reaction continued, more pore space was created and connected. The elevated pore pressure, beginning from the drained end, progressively released toward the sealed end at stage II. Consequently, reaction rate was accelerating and more pore fluid was ready to flow out. Because permeability has also increased largely at this stage, the fluid expulsion rate rose dramatically at this stage. At the final stage, although the fluid expulsion rate once again dropped down, unlike at the stage I, pore pressure excess at stage III was negligible. We will demonstrate that this low fluid expulsion reflects the dehydration reaction was nearly completed rather than halted by elevated pore pressure.

Fig. 6 illustrates the fraction of transformation of gypsum to bassanite through time. Once again our model predicts the distinct character of three-stage transformation as observed in laboratory (Fig. 6a): Dehydration was slowly at stage I due to elevated pore pressure. As pore pressure alleviated at stage II, reaction rate increased dramatically. At stage III, more than 90% of gypsum has transformed to bassanite and the reaction rate was largely reduced.

An important feature of the current simulations is that the model can capture the spatial heterogeneity as manifested by the progressive development of a reaction front. Fig. 6b shows that initially the dehydration reaction was nearly homogenous over the whole sample. Later, reaction was more concentrated in the area near the drained end where less pore pressure excess was built up than near the sealed end. This heterogeneity of transformation is so distinct at stage II that, for instance, at $t = 100$ min after initiation of dehydration, more than 90% or gypsum has transformed to bassanite near the drained end while less than 10% of dehydration reaction has completed near the sealed end. At stage III, this heterogeneity became much less distinct as most gypsum has transformed to bassanite.

The evolution of porosity on dehydrating gypsum we predicted is also consistent with microstructural

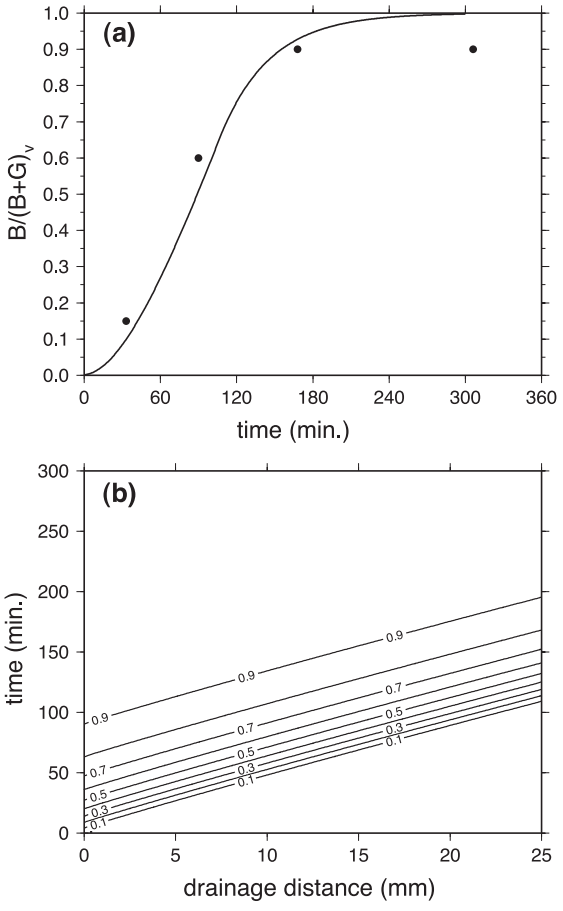

Fig. 6. The volumetric reaction ratio ($B/(B+G)$) versus time at $T = 128$ °C, $P_c = 150$ MPa and $P_0 = 10$ MPa. (a) Comparison of our simulation (solid line) with laboratory data (solid dots) from Ko et al. (1997); (b) spatiotemporal evolution of the reaction ratio. Note that a reaction front was progressively migrating toward the sealed end of the sample.

analyses except at stage I, where the measurement of Ko et al. (1997) shows abnormally high porosity (Fig. 7a). Although this apparent discrepancy may be partly attributed to the uncertainly of microstructural characterization, it may also reflect additional pore space created by hydraulic fracturing due to the rapidly elevated pore pressure generated at this stage as discussed earlier. Nevertheless, the reasonable agreement between our model and observed porosity at the subsequent stages suggests that most of the hydraulic fractures might have been closed during the stage II as a result of quickly alleviated pore pressure as shown

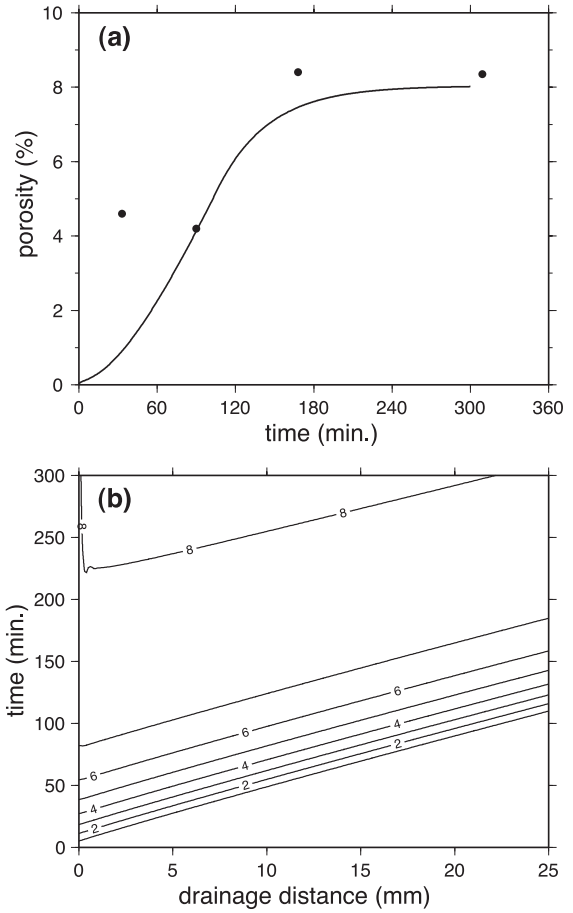

Fig. 7. Porosity versus time at $T=128$ °C, $P_c=150$ MPa and $P_0=10$ MPa. (a) Comparison of our simulation (solid line) with laboratory data (solid dots) from Ko et al. (1997); (b) spatiotemporal evolution of porosity. Note that pore space progressively decreased toward the sealed end of the sample. This heterogeneity of porosity is most noticeable in the period of $t=20$ min to $t=150$ min. Also note that the bend of contour line of porosity 8% in (b) may be a numerical artifact as all porosities above 8% are actually extremely close to 8%.

in Fig. 5. However, a rapid increase of net porosity at this stage suggests that the effect of closure of hydraulic fractures was overwhelmed by creating new pore space due to fast transformation of gypsum to bassanite at this stage. At stage III, much less pore space was generated as the dehydration reaction neared complete.

Fig. 7b illustrates the spatial heterogeneity of porosity through time. As one might expect, this pattern is similar to Fig. 6b as it basically reflects the heterogeneity of the transformation of gypsum in the undrained system. Our model suggests that at stage I, porosity was less than 0.5% especially in the area near the sealed end. This led to a low permeability and high pore pressure. Likewise, the heterogeneous distribution of pore space can be very distinct at stage II. For instance, at $t=100$ min after the onset of dehydration, the porosity at the drained end was over 7% while at the sealed end, it was less than 1%. Similarly, this heterogeneity became less distinct at stage III.

5. Discussion

Our numerical simulations were motivated by microstructural observations of the occurrence of a reaction front in a partially dehydrated sample. In her thesis (Plate 11.1. p167), Stretton (1996) documented unequivocally a sharp reaction front, which separates bassanite (near the drained end) from gypsum in a hydrostatic dehydration experiment on Volterra gypsum at 126 °C and confining pressure of 200 MPa. In a series of three experiments at 110 °C, confining pressure of 60 MPa and pore pressure of 10 MPa, Miller et al. (2003) observed the progressive migration of the reaction front from the drained end toward the sealed end of the sample. As illustrated in Figs. 6 and 7, by incorporating dehydration kinetics, our continuum model can reproduce the key attributes of these spatial heterogeneities. Nevertheless, it should be pointed out that there are significant uncertainties associated with the kinetic model and hydromechanical relations, as noted also in similar recent studies (Ague et al., 1998; Ague and Rye, 1999; Balashov and Yardley, 1998).

Instead of a continuum model, one can resort to a cellular automaton model, which allows one to conveniently incorporate statistical distribution of physical properties and to model localization of failure and channeling of fluid flow (Miller et al., 2003). In such a discrete model, pore pressure excess develops under undrained condition as a discrete jump in response to dehydration that occurs during a given time step. Our analytic results here (such as Eq. (12c)) clarify how the poroelastic moduli and reaction rates control the pore pressure evolution and place limits on the characteristic time scales involved in such an idealized model.

The discrete model also has an intrinsic limitation in that permeability is binarized in the sense that this important hydrological property is idealized as either zero or infinite. During pore pressure development, the discrete elements are all undrained with zero permeability. When the pore pressure has attained a threshold, then the permeability instantaneously switches to become infinite to allow hydraulic connectivity among the discrete cells. Consequently time scales and phenomena related to hydraulic diffusion are neglected.

One may also argue that since the simpler model of Wong et al. (1997) is capable of delineating the spatiotemporal evolution of pore pressure in a nominally drained system, the progressive development of reaction can be analyzed more simply by an equilibrium model without kinetics, using the equilibrium boundary (as functions of pore pressure) under isothermal conditions to map out the reaction front. However, since the spatial heterogeneity in reaction progress arises precisely because of kinetics, such a ''decoupled'' approach is not self-consistent: it appeals to kinetics to establish the spatial distribution of pore pressure and then conveniently forgets about kinetics when mapping out the reaction front. To be consistent, the coupling and feedback among dehydration progress, fluid drainage and porosity production have to be explicitly analyzed, even though it necessarily introduces additional mathematical complexity.

While our continuum model is in qualitative agreement with experimental and microstructural observations, its further refinement would require the systematic acquisition of better experimental data. Our choices for permeability, poroelastic moduli, reaction order and other dehydration kinetics parameters are comparable to values measured in gypsum, serpentinite and other dehydrating systems. Nevertheless, there is a paucity of high-quality data that have been obtained for input into analysis as what we conducted here.

While we have limited our simulations here to gypsum under isothermal condition, it is clearly of interest to extend the analysis to a metamorphic and tectonic environment that involves other dehydrating systems under variable temperature and pressure conditions. We have also focused on the feedback between dehydration kinetics and fluid transport in a system characterized by a poroelastic, brittle rheology, while other recent studies (e.g., Connolly, 1997; Balashov and Yardley, 1998) considered the other end-member of a solid matrix that creeps obeying a ductile rheology. A future challenge would be to develop a comprehensive model that captures the interplay of dehydration kinetics, fluid percolation and rock rheology under conditions at which the rock can undergo the brittle–ductile transition.

Acknowledgements

We have benefited from discussions with Iona Stretton and Wouter van der Zee on their microstructural observations on reaction front. We would like to thank Jamie Connolly and Dave Olgaard for furnishing us a preprint. Dr. Guy Simpson and an anonymous reviewer provided critical comments that have guided us in revising the manuscript. The research in Taiwan is partially supported by the National Science Council under grant NSC 88-2116-M-194-003 and at Stony Brook is partially supported by the National Science Foundation under grant EAR98005072.

References

Ague, J.J., Rye, D.M., 1999. Simple models of CO_2 release from metacarbonates with implications for interpretation of directions and magnitudes of fluid flow in the deep crust. J. Petrol. 40, 1443–1462.

Ague, J.J., Park, J., Rye, D.M., 1998. Regional metamorphic dehydration and seismic hazard. Geophys. Res. Lett. 25, 4221–4224.

Balashov, V.N., Yardley, W.D., 1998. Modeling metamorphic fluid flow with reaction–compaction–permeability feedbacks. Am. J. Sci. 298, 441–470.

Bredehoeft, J.D., Hanshaw, B.B., 1968. On the maintenance of anomalous fluid pressures: I. Thick sedimentary sequences. Geol. Soc. Amer. Bull. 79, 1097–1106.

Bredehoeft, J.D., Norton, D.L., 1990. The Role of Fluids in Crustal Processes. National Academy Press, Washington, DC. 170 pp.

Connolly, J.A.D., 1997. Devolatilization-generated fluid pressure and deformation-propagated fluid flow during prograde regional metamorphism. J. Geophys. Res. 102, 18149–18173.

Connolly, J.A.D., Cesare, B., 1993. C-O-H-S fluid composition and oxygen fugacity in graphitic metapelites. J. Metamorph. Geol. 11, 379–388.

David, C., Wong, T.-f., Zhu, W., Zhang, J., 1994. Laboratory measurement of compaction-induced permeability change in porous rock: implications for the generation and maintenance

of pore pressure excess in the crust. Pure Appl. Geophys. 143, 425–456.

Davis, J.H., 1999. The role of hydraulic fractures and intermediate-depth earthquakes in generating subduction-zone magmatism. Nature 398, 142–145.

Domenico, P.A., Palciauskas, V.V., 1988. The generation and dissipation of abnormal fluid pressures in active depositional environments. In: Back, W., Rosenhein, J.S., Seaber, P.R. (Eds.), The Geology of North America. Hydrogeology, vol. 0–2. The Geological Society of America, Boulder, Colorado, pp. 435–445.

Etheridge, M.A., Wall, V.J., Cox, S.F., Vernon, R.H., 1984. High fluid pressures during regional metamorphism and deformation: implications for mass transport and deformation mechanisms. J. Geophys. Res. 89, 4344–4358.

Hanshaw, B.B., Bredehoeft, J.D., 1968. On the maintenance of anomalous fluid pressures: II. Source layer at depth. Geol. Soc. Amer. Bull. 79, 1107–1122.

Heard, H.C., Rubey, W.W., 1966. Tectonic implications of gypsum dehydration. Geol. Soc. Amer. Bull. 77, 741–760.

Ingebritsen, S.E., Sanford, W.E., 1998. Groundwater in Geologic Processes. Cambridge Univ. Press, New York. 341 pp.

Kirby, S.H., Engdahl, E.R., Denlinger, R., 1996. Intraslab earthquake and arc volcanism: dual physical expressions of crustal and uppermost mantle metamorphism in subducting slabs. In: Bebout, G.E., Scholl, D., Kirby, S.H. (Eds.), Subduction: Top to Bottom. American Geophysical Union, Washington, DC, pp. 195–214.

Ko, S.-C., Olgaard, D.L., Wong, T.-f., 1997. Generation and maintenance of pore pressure excess in a dehydrating system: 1. Experiments and microstructural observations. J. Geophys. Res. 102, 825–839.

Lasaga, A.C., Rye, D.M., 1993. Fluid flow and chemical reaction kinetics in metamorphic systems. Am. J. Sci. 293, 361–404.

McConnell, J.D.C., Astill, D.M., Hall, P.L., 1987. The pressure dependence of the dehydration of gypsum to bassanite. Mineral. Mag. 51, 453–457.

Miller, S.A., van der Zee, W., Olgaard, D.L., Connolly, J.A.D., 2003. A fluid-pressure feedback model of dehydration reactions: experiments, modeling and application to subduction zones Tectonophysics, this volume.

Moore, J.C., Vrolijk, P., 1992. Fluids in accretionary prisms. Rev. Geophys. 30, 113–136.

Murrell, S.A.F., 1985. Aspects of relationships between deformation and prograde metamorphism that causes evolution of water. In: Thompson, A.B., Bubie, D.C. (Eds.), Metamorphic Reactions, Kinetics, Textures and Deformation. Adv. Phys. Geochem., vol. 4. Springer-Verlag, Berlin, pp. 211–241.

Murrell, S.A.F., Ismail, I.A.H., 1976. The effect of decomposition of hydrous minerals on the mechanical properties of rocks at high pressures and temperatures. Tectonophysics 31, 207–258.

Olgaard, D.L., Ko, S.-C., Wong, T.-f., 1995. Deformation and pore pressure in dehydrating gypsum under transiently drained conditions. Tectonophysics 245, 237–248.

Peach, C.J., Spiers, C.J., 1996. Influence of crystal plastic deformation on dilatancy and permeability development in synthetic salt rock. Tectonophysics 256, 101–128.

Peacock, S.M., 2001. Are the lower planes of double seismic zones caused by serpentine dehydration in subducting oceanic mantle? Geology 29, 299–302.

Popp, T., Kern, H., Schulze, O., 2001. Evolution of dilatancy and permeability in rock salt during hydrostatic compaction and triaxial deformation. J. Geophys. Res. 106, 4061–4078.

Raleigh, C.B., Paterson, M.S., 1965. Experimental deformation of serpentinite and its tectonic implications. J. Geophys. Res. 70, 3965–3985.

Stretton, I.C., 1996. An Experimental Investigation of the Deformation Properties of Gypsum. PhD thesis, University of Manchester, Manchester.

Walder, J., Nur, A., 1984. Porosity reduction and crustal pore pressure development. J. Geophys. Res. 89, 11539–11548.

Wong, T.-f., Ko, S.-C., Olgaard, D.L., 1997. Generation and maintenance of pore pressure excess in a dehydrating system: 2. Theoretical analysis. J. Geophys. Res. 102, 841–852.

Zhang, S., FitzGerald, J.D., Cox, S.F., 2000. Reaction-enhanced permeability during decarbonation of calcite + quartz → wollastonite + carbon dioxide. Geology 28, 911–914.

Zhu, W., Wong, T.-f., 1999. Network modeling of evolution of permeability and dilatancy in compact rocks. J. Geophys. Res. 104, 2963–2971.